Journal of Power Sources 216 (2012) 1–4

Contents lists available at SciVerse ScienceDirect

Journal of Power Sources

journal homepage: www.elsevier.com/locate/jpowsour

Short communication

Improving the chemical compatibility of sealing glass for solid oxide fuel cells: Blocking the reactive species by controlled crystallization

Teng Zhang [a,*], Qi Zou [a], Fanrong Zeng [b], Shaorong Wang [b], Dian Tang [a], Hiswen Yang [c]

[a] College of Materials Science and Engineering, Fuzhou University, Fuzhou, Fujian 350108, China
[b] CAS Key Laboratory of Materials for Energy Conversion, Shanghai Institute of Ceramics, Chinese Academy of Sciences (SICCAS), 1295 Dingxi Road, Shanghai 200050, China
[c] Department of Materials Science and Engineering, National United University, Miao-Li 36003, Taiwan

HIGHLIGHTS

► Interfacial reaction can be reduced by controlled crystallization of sealing glass.
► Sr-containing crystalline is critical for the chemical stability of sealing glass.
► The improved chemical stability can be explained by thermodynamic models.

ARTICLE INFO

Article history:
Received 10 April 2012
Accepted 5 May 2012
Available online 26 May 2012

Keywords:
Solid oxide fuel cell
Interfacial reaction
Controlled crystallization
Chemical compatibility
Thermodynamic calculation

ABSTRACT

The chemical compatibility of sealing glass is of great importance for Solid oxide fuel cell (SOFC). In this work, the interfacial reaction between sealing glass and Cr-containing interconnect alloy is characterized by reacting Cr_2O_3 powders with a representative SrO-containing glass crystallized by different heat-treatment schedules. The crystalline structure and crystalline content of sealing glass are determined by X-ray diffraction. The results show that the fraction of Cr^{6+} decreases from 39.8 ± 1.9% for quenched glass to 8.2 ± 0.4% for glass crystallized at 900 °C for 2 h. In addition, the interfacial reaction can be further reduced with increasing crystallization temperature and time as well as the addition of nucleation agent (TiO_2). The formation of some Sr-containing crystalline phases, Sr_2SiO_4 and $Sr(TiO_3)$, contributes to the improvement of chemical compatibility of sealing glass, in agreement with the results of thermodynamic calculations.

1. Introduction

Solid oxide fuel cell (SOFC) is of great interest in recent years as a promising electro-chemical device for generating electricity from various fuels [1,2]. Compared with the rapid progress on other SOFC components [3–5], the sealing materials (primarily glasses and glass-ceramics) are becoming the bottleneck of SOFC technology. In particular, the interfacial reaction between glass-ceramic sealants and ferritic interconnects results in the formation of chromate phases, *e.g.*, $BaCrO_4$ and $SrCrO_4$, and consequently the physical separation of the sealants from the interconnects [6,7].

To reduce the chromate formation, modifications of interconnect alloys have been extensively investigated, such as pre-oxidation [8], aluminizing [9] and protective coatings [10,11]. Attention has also been focused on the chemical compatibility and thermal cycle stability of sealants [12–17]. However, the complex fixture of sealing couples restricts the precise analysis on the reaction and results in the qualitative conclusions in most studies. Our recent work reported a quantitative analysis on the model reaction between sealing glass and Cr_2O_3 powders by UV–Vis spectrum, which provides a reliable and convenient approach to evaluate the effect of different additives on the chemical compatibility of sealing glass [18].

In this paper, a representative Sr-containing sealing glass [18] was crystallized by different heat-treatment schedules as well as nucleation agent (2 mol% TiO_2) and reacted with Cr_2O_3 powders at the operational condition of SOFC. The crystalline structure and crystalline content of sealing glasses were determined by X-ray diffraction. The chemical compatibility of glass-ceramics was evaluated using the quantitative approach developed by ourselves. The relationship between the crystalline characteristics (crystalline structure and crystalline content) and the chemical compatibility of sealing glasses was then established to provide better understanding on the nature of interfacial reaction. The change in the

* Corresponding author. Tel.: +86 591 22866540; fax: +86 591 22866537.
E-mail address: Teng_zhang@fzu.edu.cn (T. Zhang).

0378-7753/$ – see front matter © 2012 Elsevier B.V. All rights reserved.
doi:10.1016/j.jpowsour.2012.05.034

chemical compatibility of sealing glass was also explained by thermodynamic calculations.

2. Experimental

A 50-g sample of glass designated 'M_0' was prepared from a batch mixture of reagent grade alkaline earth carbonates, boric acid, and various oxides to form the nominal glass composition (mole %): 26.0CaO–26.0SrO–4.0B_2O_3–44.0SiO_2. Another modified composition designated 'T_1' was prepared for comparison, with a nominal glass composition (mol%) of 25.5CaO–25.5SrO–3.9B_2O_3–2.0TiO_2–43.1SiO_2. The batches were melted in an alumina crucible at a temperature of 1500 °C for 2 h in air and the melts were then quenched on steel plates.

Glass#M_0 powders were then crushed and sieved to a particle size of 45–53 μm. The glass transition temperature (T_g) and onset crystallization temperature (T_c) of quenched glass powders were determined using differential scanning calorimetry (SDTQ600, TA, Inc.) at a heating rate of 10 °C min^{-1}. The coefficient of thermal expansion (CTE) of quenched glass was measured using dilatometer (DIL402C, NETZSCH, Inc.) at a heating rate of 5 °C min^{-1}.

Glass#M_0 were crystallized in a preheated furnace (*e.g.*, 780, 800 and 900 °C) for different time and quenched in air. The density of some crystallized samples was measured using the Archimedes method in water. The crystalline phases in crystallized samples were identified using X-ray Diffraction (XDS 2000, Scintag, Inc.). The crystalline content (weight%) in each sample was then calculated by RIQAS software (Release 4.0.0.8, Materials Data, Inc., CA). The polished surface of crystallized samples (finished by 1200 grit SiC paper) was analysed using Scanning Electron Microscopy (S-4700, Hitachi, Inc.).

A ~20-mg mixture of sealing glass and 10 weight% Cr_2O_3 powders was reacted in an alumina boat in air in the operational temperature range of SOFC for different time. The reaction product was dissolved into ~100 ml of deionized water and the absorption spectra were recorded using the UV–VIS Spectrometer (Optima 2000 DV, Perkin Elmer, Inc.). The fraction of Cr^{6+} was then calculated by fitting the measured absorption to the calibration curve. The detailed procedure of this quantitative analysis by UV–VIS spectrometer has been discussed elsewhere [18].

3. Results and discussion

Some properties of the sealing glass#M_0 are summarized in Table 1. The glass transition temperature (T_g), and onset crystallization temperature (T_c) of quenched glass are 730 ± 3 and 860 ± 3 °C, respectively. The coefficient of thermal expansion (CTE) of the sealing glass is 11.2 ± 0.3 × 10^{-6} K^{-1}, in the range of design target (11–13 × 10^{-6} K^{-1}) for minimizing the CTE mismatch in SOFC stacks [6]. The crystalline content of samples, crystallized for 2 h, increases from 26 ± 5 to 43 ± 5 and to 68 ± 5 weight% when the crystallization temperature increases from 780 to 800 and to 900 °C. In addition, the density of samples crystallized at 780, 800 and 900 °C for 2 h are 3.00 ± 0.03, 3.08 ± 0.03 and 3.10 ± 0.03 g cm^{-3}, respectively.

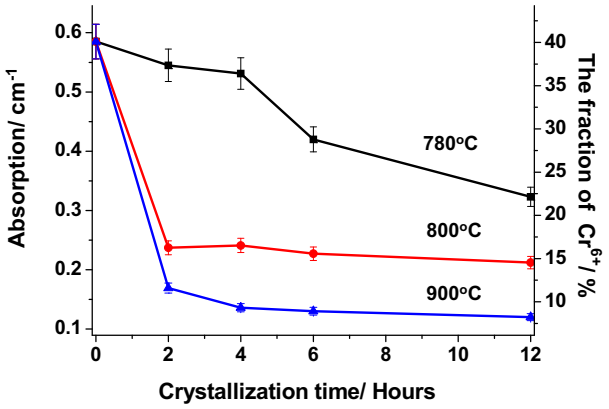

Fig. 1. The absorption of Cr^{6+} (left *Y*-axis) and the fraction of Cr^{6+} (right *Y*-axis) in the reaction couples between Cr_2O_3 and glass#M_0 powders, after reacting in air at 750 °C for 30 min, as a function of crystallization time.

Fig. 1 shows the absorption of Cr^{6+} (left *Y*-axis) and the fraction of Cr^{6+} (right *Y*-axis) in the reaction couples between Cr_2O_3 and glass#M_0 powders, after reacting in air at 750 °C for 30 min, as a function of crystallization time. It is clear that the fraction of Cr^{6+} decreases from 39.8 ± 1.9% for quenched glass to 8.2 ± 0.4% for glass crystallized at 900 °C for 2 h. In addition, the fraction of Cr^{6+}, in samples crystallized for 2 h, decreases from 33.7 ± 1.6 to 16.2 ± 0.7 and to 11.6 ± 0.5% when the crystallization temperature increases from 780 to 800 and to 900 °C. Moreover, the fraction of Cr^{6+}, in samples crystallized at 900 °C, decreases from 11.6 ± 0.5 to 8.9 ± 0.2 and to 8.2 ± 0.2% when the crystallization time increases from 2 to 6 and to 12 h.

Fig. 2 shows the XRD patterns of glass#M_0 after crystallization for 2 h. The main phases in all samples are identified to be Sr_2SiO_4 (JCPDS Card No. 38-0271), Ca_2SiO_4 (JCPDS Card No. 36-0642) and $CaSiO_3$ (JCPDS Card No. 43-1460). The ratio of the intensity of (220) plane in Sr_2SiO_4 ($2\theta = 31.3°$, referred to as I_1) to that of (036) plane in Ca_2SiO_4 ($2\theta = 39.5°$, referred to as I_2) increases from 0.84 to 2.18 and to 8.76 when the crystallization temperature increases from 780 to 800 and to 900 °C, indicating that the increase of Sr_2SiO_4 content is faster than that of Ca_2SiO_4 content with increasing crystallization temperature.

Fig. 3 shows the SEM images for glass#M_0 after crystallization. Few crystalline can be observed in glass crystallized at 780 °C for 2 h (in Fig. 3a); whereas, numerous crystalline in sample crystallized at 900 °C for 2 h (in Fig. 3b) confirms the high crystalline content of this sample, in agreement with the quantitative XRD results in Table 1. Considering the greater crystalline content (in Table 1 and Fig. 3) and the faster increase of Sr_2SiO_4 content than that of Ca_2SiO_4 content at higher temperature (in Fig. 2), one can conclude that the Sr_2SiO_4 content increases with increasing crystallization temperature, consistent with the reduction of chromate formation under identical condition (in Fig. 1).

Fig.4a shows the absorption of Cr^{6+} (left *Y*-axis) and the fraction of Cr^{6+} (right *Y*-axis) in the reaction couples between Cr_2O_3 and glass#M_0 powders, after reacting in air at 800 °C, as a function of reaction time. To further clarify the effect of crystallization on the

Table 1
Properties of the sealing glass#M_0.

T_g (°C)	T_c (°C)	T_d (°C)	CTE (×10^{-6} K^{-1})	Conditions for crystallization	Crystalline content (weight%)	Density (g cm^{-3})
730 ± 3	806 ± 3	750 ± 3	11.2 ± 0.3	780 °C, 2 h	26 ± 5	3.00 ± 0.03
				800 °C, 2 h	43 ± 5	3.08 ± 0.03
				900 °C, 2 h	68 ± 5	3.10 ± 0.03

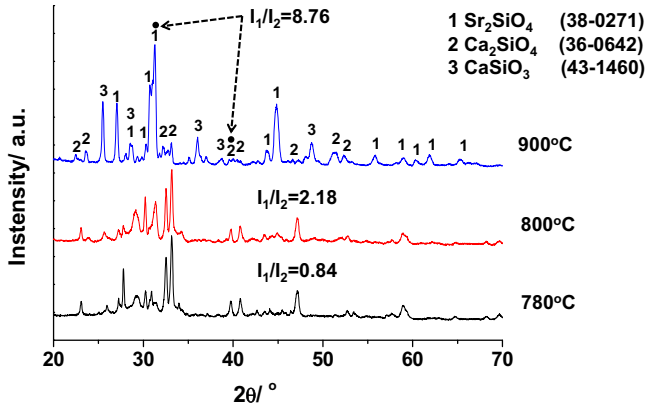

Fig. 2. XRD patterns of glass#M_0 after crystallization at different temperatures for 2 h.

chemical compatibility of sealing glass, the reaction between Cr_2O_3 and glass#T_1 powders was also characterized under the identical condition for comparison. It is clear that the fraction of Cr^{6+} decreases from 54.2 ± 2.7% for glass#M_0 to 36.4 ± 1.7% for glass#T_1, after reacting at 800 °C for 7 h Fig. 4b shows the XRD patterns of sealing glasses after crystallization at 900 °C for 2 h. The main phases in both glasses are similar, except for the formation of $Sr(TiO_3)$ (JCPDS Card No.86-0179) with the addition of TiO_2. In addition, the ratio of I_1 to I_2 increases from 8.76 for glass#M_0 to 22.75 for glass#T_1, indicating the faster increase of Sr_2SiO_4 content of glass#T_1 with the addition of TiO_2.

Fig.5a shows the Gibbs energy changes for possible reactions at 800 °C as a function of partial pressure of oxygen. The reaction between Sr^{2+} ions in quenched glass and Cr_2O_3 can be described as following:

$$SrO_{(glass)} + 0.5Cr_2O_{3(solid)} + 0.75O_2 \leftrightarrow SrCrO_{4(solid)} \quad (1)$$

Similarly, the reaction between Sr^{2+} ions in crystallized glass and Cr_2O_3 can be described as following:

$$0.5Sr_2SiO_{4(crystalline)} + 0.5Cr_2O_{3(solid)} + 0.75O_2 \leftrightarrow SrCrO_{4(solid)} + 0.5SiO_{2(solid)} \quad (2)$$

$$Sr(TiO_3)_{(crystalline)} + 0.5Cr_2O_{3(solid)} + 0.75O_2 \leftrightarrow SrCrO_{4(solid)} + TiO_{2(solid)} \quad (3)$$

The activity of SrO is simplified to be its molar fraction in glass (0.26) in present work, assuming the glass is ideal solution. It is

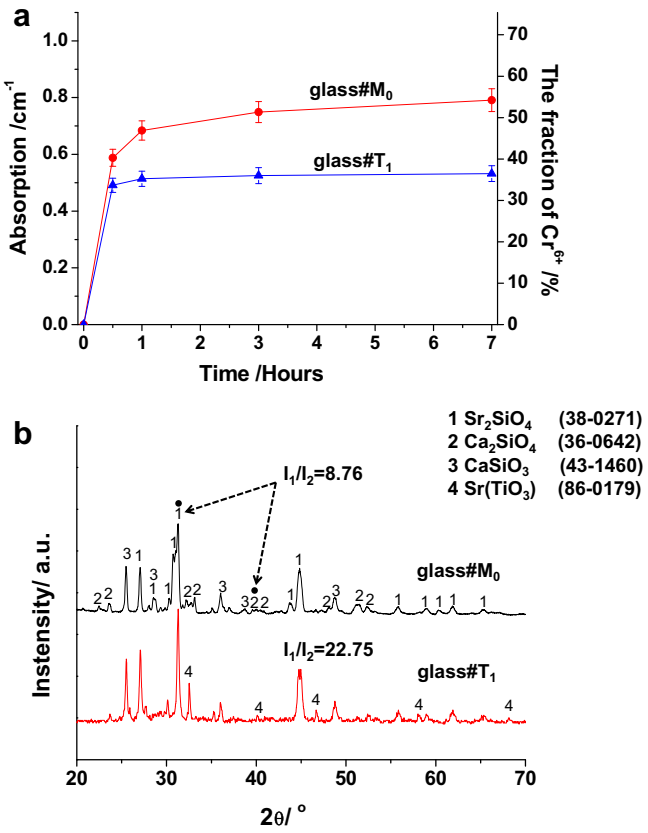

Fig. 4. (a) The absorption of Cr^{6+} (left *Y*-axis) and the fraction of Cr^{6+} (right *Y*-axis) in the reaction couples between Cr_2O_3 and glass powders (glass#M_0 and #T_1), after reacting in air at 800 °C, as a function of reaction time, and (b) XRD patterns of sealing glasses (glass#M_0 and #T_1) after crystallization at 900 °C for 2 h.

clear that the Gibbs energy changes for possible reactions at 800 °C decrease with increasing partial pressure of oxygen. For example, the Gibbs energy change of reaction (1) at 800 °C on the anode (in forming gas, $PO_2 = 10^{-16}$ atm) and cathode side (in air, $PO_2 = 0.2$ atm) are 105 and −133 kJ mol^{-1}, respectively. Therefore, thermodynamic studies on the interfacial reaction of SOFC have been focused on the cathode side (in air) [19].

The Gibbs energy changes for possible reactions on the cathode side (in air) were then calculated as a function of temperature, as shown in Fig. 5b. The Gibbs energy changes for possible reactions on the cathode side increase with increasing temperature. For example, the Gibbs energy change of reaction (1) on the cathode side increases from −146 to −133 kJ mol^{-1} when the temperature increases from 700 to 800 °C. It is worth noting that the Gibbs

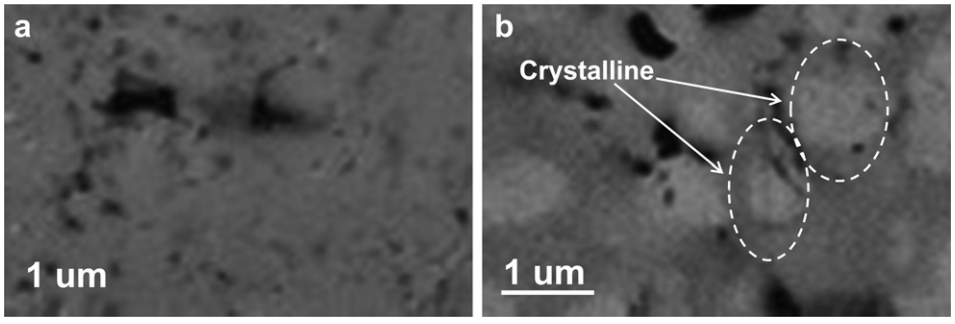

Fig. 3. SEM images for glass#M_0 (a) crystallized at 780 °C for 2 h and (b) crystallized at 900 °C for 2 h.

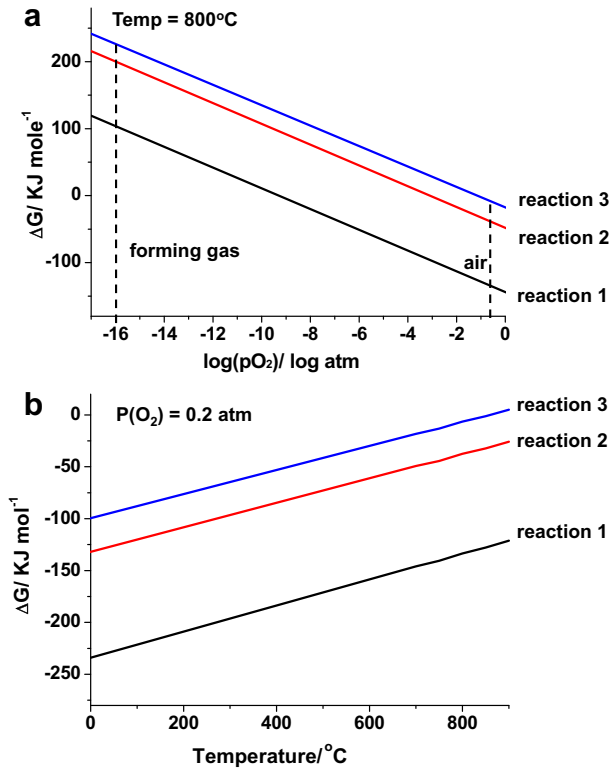

Fig. 5. Gibbs energy changes for possible reactions (a) at 800 °C as a function of partial pressure of oxygen and (b) on the cathode side (in air) as a function of temperature.

energy change on the cathode side (PO_2 = 0.2 atm) at 800 °C decreases from −133 for reaction (1) to −37 for reaction (2) and to −7 mol^{-1} for reaction (3).

Therefore, the Sr^{2+} ions in crystalline (Sr_2SiO_4 in reaction (2) as well as $Sr(TiO_3)$ in reaction (3)) is more stable than that in glass matrix (SrO in reaction (1)) in the operational temperature range of SOFC based on thermodynamic calculations (in Fig. 5). The formation of Sr-containing crystalline phases, Sr_2SiO_4 and $Sr(TiO_3)$, contributes to the significant reduction of chromate formation in the reaction couple between sealing glass and Cr_2O_3 powders by controlled crystallization (in Figs. 1 and 4). In addition, the effect of densification on the reaction extent can be excluded considering the negligible change in density after crystallization (in Table 1).

4. Conclusions

The interfacial reaction between sealing glass and Cr-containing interconnect alloy can be reduced by controlled crystallization. The formation of Sr-containing crystalline phases, Sr_2SiO_4 and $Sr(TiO_3)$, contributes to the significant improvement of chemical compatibility of sealing glass, which is also confirmed by thermodynamic calculations. The founding on the relationship between the chemical compatibility and the crystalline structure of sealing glass in present work provides an effective and practical approach for reducing the interfacial reaction and improving the performance of SOFC. In addition, the idea about blocking reactive species in stable crystalline can also be applied to similar circumstances in which chemical compatibility is critical.

Acknowledgements

The authors gratefully acknowledge the financial support of the National Natural Science Foundation of China (No. 51102045), the Ph.D. Programs Foundation of Ministry of Education of China (No. 20103514120006), funds for Distinguished Young Scientists from the Fujian Education Department (No. JA11007) and the funding (type A) (No. JA09020) from the Fujian Education Department of China. The authors also would like to thank Dr. Bingxi Wang for useful discussion.

References

[1] H. Qin, Z. Zhu, Q. Liu, Y. Jing, R. Raza, S. Imran, M. Singh, G. Abbas, B. Zhu, Energy Environ. Sci. 4 (2011) 1273–1276.
[2] Z. Shao, C. Zhang, W. Wang, C. Su, W. Zhou, Z. Zhu, H.J. Park, C. Kwak, Angew. Chem. Int. Ed. 50 (2011) 1792–1797.
[3] M. Liu, J. Gao, X. Liu, G. Meng, Int. J. Hydrogen Energy 36 (2010) 13741–13745.
[4] J.C. Ruiz-Morales, D. Marrero-Lopez, M. Galvez-Sanchez, J. Canales-Vazquez, C. Savaniu, S.N. Savvin, Energy Environ. Sci. 3 (2010) 1670–1681.
[5] T. Wei, Q. Zhang, Y.-H. Huang, J.B. Goodenough, J. Mater. Chem. 22 (2012) 225–231.
[6] J.W. Fergus, J. Power Sources 147 (2005) 46–57.
[7] M.K. Mahapatra, K. Lu, J. Power Sources 195 (2010) 7129–7139.
[8] Y.-S. Chou, J.W. Stevenson, P. Singh, J. Power Sources 184 (2008) 238–244.
[9] Y.-S. Chou, J.W. Stevenson, P. Singh, J. Power Sources 185 (2008) 1001–1008.
[10] B. Hua, J. Pu, W. Gong, J. Zhang, F. Lu, L. Jian, J. Power Sources 185 (2008) 419–422.
[11] M.K. Mahapatra, K. Lu, Int. J. Hydrogen Energy 35 (2010) 11908–11917.
[12] Y.-S. Chou, E.C. Thomsen, R.T. Williams, J.P. Choi, N.L. Canfield, J.F. Bonnett, J.W. Stevenson, A. Shyam, E. Lara-Curzio, J. Power Sources 196 (2011) 2709–2716.
[13] Y.-S. Chou, E.C. Thomsen, J.P. Choi, J.W. Stevenson, J. Power Sources 197 (2012) 154–160.
[14] T. Jin, K. Lu, J. Power Sources 195 (2010) 4853–4864.
[15] F. Smeacetto, A. Chrysanthou, M. Salvo, T. Moskalewicz, F. D'Herin Bytner, L.C. Ajitdoss, M. Ferraris, Int. J. Hydrogen Energy 36 (2011) 11895–11903.
[16] A. Goel, D.U. Tulyaganov, V.V. Kharton, A.A. Yaremchenko, J.M.F. Ferreira, J. Power Sources 195 (2010) 522–526.
[17] Z. Dai, J. Pu, D. Yan, B. Chi, L. Jian, Int. J. Hydrogen Energy 36 (2011) 3131–3137.
[18] T. Zhang, H. Zhang, G. Li, H. Yung, J. Power Sources 195 (2010) 6795–6797.
[19] T. Zhang, R.K. Brow, W.G. Fahrenholtz, S.T. Reis, J. Power Sources 205 (2012) 301–306.